Hydrogen based solutions to help electrical grid management

Application to the Terceira Island case

Luiz Carlos Santos de Jesus
luiz.jesus@tecnico.ulisboa.pt
Instituto Superior Técnico, Universidade de Lisboa, Portugal
November 2021

Abstract

The need for decarbonization has become an urgent objective being pursued across borders and sectors. The energy sector has been one example to follow, with the penetrations of renewable energy sources increasing year after year and already having an impact on carbon emissions. Despite their benefits, as these penetration levels grow, grid stability has been affected. Part of this instability is caused by the different type of connection to the grid used by most renewable energy sources. These converter connected technologies do not contribute to the grid's inertia the same way synchronous generators do.

Focusing on the behavior of the system's frequency, a Matlab/Simulink based model of the Portuguese Terceira Island is created to assess the potential benefits of using hydrogen technologies to provide grid services. Two different scenarios are analyzed, the system's frequency response to large imbalances and to steady-state imbalances stemming from load and wind power forecasting errors. The results reflect on how the frequency behavior is affected by the amount of system's inertia, synchronous generators characteristics and the presence of electrolyzers and fuel cells, with new metrics being introduced to compare the frequency's reaction to each.

Keywords: Renewable Energy Sources; Hydrogen Technologies; Frequency Control; Large imbalances; Steady-state imbalances.

1. Introduction

Renewable energy sources (RES) have been the leading effort to decarbonize the energy sector, having not just a direct impact on sustainability through the substitution of carbon-based power sources, but also through allowing the process of electrification across many sectors. For these reasons RES have been adopted at increasing rates and are showing positive results. With their large uptake and the increasing electricity demand, the energy sector is in a clear transition period. This transition is, at the surface level, simply based on substituting carbon-based power sources by renewable ones, but, even just at a technical level, the different characteristics of these technologies makes this transition much more complex than it seems.

The electricity system is based on a constant balance between power demand and supply, whose state can be evaluated through the system's frequency, the frequency shared by all connected machines. Deviations from the frequency's nominal value can have negative implications and even damage grid systems. The differences in connection to the grid between technologies, with traditional thermoelectric power centrals being synchronously connect and wind and solar sources being converter connected, has caused changes to an important frequency stability parameter, the inertia constant. Simultaneously the unpredictable and uncontrollable nature of renewable resources like wind and solar energy, has led to an increase in uncertainty, being reflected in steady-state imbalances caused by load and power forecasting errors.

Many solutions have been studied, with the one presented here being comprised of using hydrogen-based technologies, to perform grid frequency balancing services.

A grid model is developed here to test two different scenarios with three configurations. The model created will be based on the Terceira Island of the Portuguese autonomous region of Azores. This archipelago already has a defined 2030 energy strategy [1] with targets that would be helped by a project like the one presented here. For a long time the thermoelectric central of Belo Jardim, with its 61.116 MW, has been the backbone of electricity production in the island, but the investments done in RES have introduced 12.6 MW of wind power and 3.5 MW of geothermal power since 2008. These were the power sources considered in the model.

In Chapter 2, the state of the art of key research topics tackled here is presented, giving an overview of RES, frequency control mechanisms and hydrogen technologies. Chapter 3 describes the grid model developed and the novel metric proposed. The simulation results for each of the

scenarios and configurations tested are presented and analyzed in Chapter 4. Finally, Chapter 5 gathers the conclusions and final remarks from the work performed.

2. State of the art

2.1. Renewables

Currently the global penetration of RES reached 27% in 2019 [23], causing a 3.1% reduction in non-abated coal. This growth is expected to continue with the addition of 1 123 GW of new solar and wind capacity between 2020 and 2025 [24], but still needs to be more pronounced to follow the Sustainable Development Scenario set by the International Energy Agency (IEA) [23].

Widén et al. (2015) [2] present an overview of the research on the topics of variability and power forecasts, pointing to the need of collaboration and standardized comparative studies across approaches and technologies. The volatility of these sources has also led to the curtailment of power, part of it being caused by set stability limits. Villamor et al. (2020) [5] modeled Great Britain's unit commitment and economic dispatch under conditions of high RES penetration, estimating that an increase in flexibility in the balancing grid services would avoid 75 to 88% of curtailment. Adding, Makolo et al. (2021) [6] evaluated the impact of lower stability characteristics resulting from the increase presence of RES. The conclusions pointed to largely negative correlation, and [4] pointed to how this can become a limiting factor in further developments.

Different types of solutions to the increased instability are being researched. [7] presented a 1 MW Li-ion battery energy storage system with three different operation strategies to increase system stability in small, isolated grid. Choosing another approach [8] pointed to the best solution being simply overbuilding RES. Similarly, to this study, [9] covered the possibility of using hydrogen storage technologies to mitigate variability of RES.

2.2. Grid services

In electrical grids the supply and demand sides must balance each other at every moment, and its machines share a common frequency that is used as a metric for that balance. This grid frequency must be kept close to its nominal value to avoid damages to the connected machines. An increased in power demand which leads the grid's frequency to go down, will thus force the grid services to respond. This frequency balance is assured by three groups divided by their specific focus, the Frequency Containment Reserve (FCR) which acts in a small window of time, 30 seconds, to stop the growth of frequency deviations and quickly reestablish power equilibrium, after that the Frequency Restoration Reserve (FRR) is activated to bring the system's frequency back to its nominal value, in case of persistent imbalances, the manually activated FRR (maFRR) can be activated. The focus of this work will be on the FCR response.

The markets to participate in these services has been more recently trying to adapt to the changes in the grid, allowing more players, changing their bid structures and seeking more flexible players. As a consequence, the viability of using hydrogen-based options has increased [10].

2.3. Hydrogen Technologies

Electrolyzers (EL) and fuel cells (FC) are electrochemical devices who, respectively, use electricity and water to generate hydrogen, and use hydrogen and oxygen to generate electricity.

Electrolyzers

The endothermic reaction of the electrolysis reaction is presented in equation 1 [11,12]. The exact details of this reaction change according to the EL technology, varying electrolytes, materials, catalysts, charge carriers, and others, leading to different characteristics between technologies, as the operations pressure and temperature, the process efficiency, the production rate, the hydrogen purity and the power response times.

$$H_2O \rightarrow H_2 + \frac{1}{2}O_2 \quad \Delta H = -288\ kJ.mol^{-1} \quad (1)$$

At this moment the EL technologies most covered in research are the Alkaline EL (AEC) [11,13,14], the Proton Exchange Membrane EL (PEMEC) [11,13,14] and the Solid Oxide EL (SOEC) [11,13-15]. Comparing the details of each of these and their current state of development, the PEMEC was the one determined to be more adequate for the combination with RES, due to their higher flexibility, rapid response times, high efficiency and stage of development.

Fuel cells

The categorization of FC can be done by the fuel used, the electrolyte or the operation temperature. From the most developed technologies: proton exchange membrane FC (PEMFC), alkaline FC (AFC), direct methanol FC (DMFC), phosphoric acid FC (PAFC), molten carbonate FC (MCFC), and solid oxide FC (SOFC), who have very distinct operations, the most suited for coupling with RES is the PEMFC, for its

high-power density, high efficiency, low working temperature, and ability to quickly regulate its power output [9.10, 9.33, 9.38].

3. Methods

A simple model of Terceira's grid was developed considering the synchronous generations, both carbon-based and from geothermal energy, the wind power generation and island's load. Additionally, models of the electrolyzer and fuel cell systems were developed and added into the grid. The system modeled will have three configurations: the simple configurations, comprised of wind and synchronous power sources and load, the electrolyzer configuration which adds the electrolyzer systems to the simple configurations, and the fuel cell configurations, which also adds the fuel cells to the electrolyzer configurations.

The functioning of the model can be divided into three phases, the input, the deviation and the response phase.

3.1. Input

3.1.1. Synchronous Generators

In the input phase the load and wind speed data are introduced in the model. These are direct inputs but also used to calculate the forecasted synchronous power, using equation 2. Where P_{sf}, P_{lf} and P_{wf} stand respectively for the forecasted synchronous power, load and wind power.

$$P_{sf} = P_{lf} - P_{wf} \quad (2)$$

The synchronous machines dynamic behavior was modeled through the block diagram presented in Figure 1, with a maximum power output equal to the summed capacity of considered sources, and a minimum equal to 10% of that, a considered maximum ramp rate of 3 percent, and a response delay of 0.4 seconds.

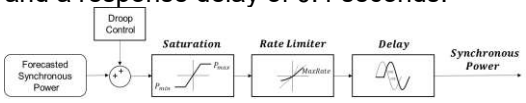

Figure 1 - Synchronous generators dynamic behavior diagram.

3.1.2. Wind Power

The wind power generation was calculated using wind speed data from the SOLCAST [25] platform. Equation 3 is used, to estimate the wind speed at hub height, applying Prandtl's law, with z_h being the hub's height, z_1 the measurements height, z_0 the roughness length, defined following Plant's classes, and $u(z_h)$, $u(z_1)$ and $u(z_0)$ the corresponding velocities.

$$u(z_h) = u(z_1) * \frac{\ln\left(\frac{z_h}{z_0}\right)}{ln\left(\frac{z_1}{z_0}\right)} \quad (3)$$

The design of the wind turbines defines four wind speed operation ranges. The wind power output at each range can be calculated with equation 4. For this 3-bladed turbine model the rotor height is 55 m, the diameter is 44 m, the rated power is 0.9 MW and the $u_{cut\,in}$, u_{rated} and $u_{cut\,out}$ are, respectively 3, 16.5 and 34 m/s.

$$\begin{cases} P = 0 & u < u_{cut\,in} \\ P = \frac{Cp.\rho.(\pi R^2).u^3}{2} & u_{cut\,in} < u < u_{rated} \\ P = P_{rated} & u_{cut\,out} < u < u_{rated} \\ P = 0 & u > u_{cut\,out} \end{cases} \quad (4)$$

3.1.3. Hydrogen Systems

The electrolyzer and fuel cells models are based on the models developed by [16] and [17], respectively. The models used are voltage models that based on the overpotentials of each cell calculate a cell's polarization curve. From there, the stack's power profile was estimated.

3.1.3.1. Electrolyzer

The electrolyzer reversible cell potential, E_0, represents the minimum potential difference between the electrodes necessary for the water splitting reaction to occur. As there is no thermal energy being supplied, this must all be provided by the electrical source. The minimum potential is thus the thermoneutral voltage, expressed in equation 5, where ΔH_R is the entire energy needed for the reaction and, n and F are the number of electron moles involved and the Faraday constant.

$$E_{th} = \frac{\Delta H_R}{nF} \quad (5)$$

The cell's open circuit voltage is calculated using the Nernst equation 6, with R being the universal gas constant, T_{el} the electrolyzer temperature, and p_{H_2},p_{O_2}, p_{H_2O} the partial pressures of hydrogen, oxygen and water.

$$V_0 = E_{th} + \frac{RT_{el}}{2F} \ln\left(\frac{p_{H_2}\sqrt{p_{O_2}}}{p_{H_2O}}\right) \quad (6)$$

The considered overpotentials caused by the reaction processes at the cell are the activation overpotential, caused by the loss of potential due to the activation of the electrochemical reactions, calculated with Butler-Volmer's equation 7; the concentration overpotential resulting from the limits of mass transport, calculated with equation 8; and the ohmic overpotential caused by the materials resistance, expressed through equation 9.

$$V_{act} = \frac{RT_{el}}{n\alpha_{an}F} \sinh^{-1}\left(\frac{i}{2i_{0,an}}\right) + \\ + \frac{RT}{n\alpha_{ca}F} \sinh^{-1}\left(\frac{i}{2i_{0,ca}}\right) \quad (7)$$

$$V_{conc} = -\frac{RT_{el}}{nF} \ln\left(1 - \frac{i}{i_{lim}}\right) \quad (8)$$

$$V_{ohm} = \frac{\delta}{\sigma} i \quad (9)$$

In these equations i is the cell's current density, α_{an} and α_{ca} are the anodic and cathodic charge transfer coefficients, $i_{o,an}$ and $i_{o,ca}$ are the exchange current densities at the anode and cathode, i_{lim} is the maximum current density of the electrolyzer, δ is the membrane thickness, and its conductivity is σ, calculated with equation 10, where λ is the membrane's water content.

$$\sigma = (5.139\lambda - 3.26)10^{-3} * \\ * exp\left[1268\left(\frac{1}{303} - \frac{1}{T_{el}}\right)\right] \quad (10)$$

The values for all these properties are given in Table 1. The electrolyzer's polarization curve, resulting from the combined action of these overpotentials, expressed in equation 11, is displayed in Figure 2.

$$V_{cell} = V_0 + V_{act} + V_{conc} + V_{ohm} \quad (11)$$

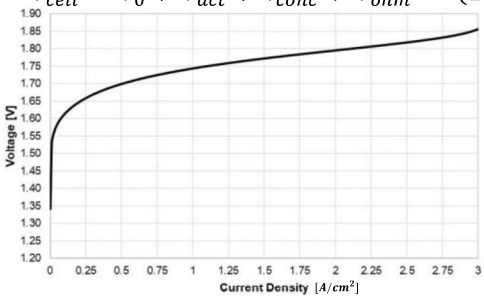

Figure 2-Modeled electrolyzer cell polarization curve.

3.1.3.2. Fuel Cell

Fuel cells also have a reversible cell potential, E_0, and an open circuit voltage, V_{th}, presented in equation 12, that now represent the voltage that obtained if no losses were present in a situation where thermal energy is provided and one where it is not.

$$V_{th} = E_0 + \left(T_{fc} - T_{ref}\right)\frac{\Delta s^0}{nF} \quad (12)$$

In the same way open-circuit voltage, equation 13, is equivalent to the amount of electricity released at a different state from standard operation conditions.

$$V_0 = V_{th} + \frac{RT_{fc}}{2F}\ln\left(p_{H_2}\sqrt{p_{O_2}}\right) \quad (13)$$

In fuel cells the overpotentials will limit the amount of power that can be produced. Identically to PEM electrolyzers the overpotentials that are most predominant are the activation, the concentration and the ohmic overpotentials, the expressions used to model these are expressed bellow in equations 14-16. The values considered for all these properties are presented in Table 1.

$$V_{act} = \frac{RT_{fc}}{\alpha_{an}F} ln\left(\frac{i}{i_{0,an}}\right) + \frac{RT_{fc}}{\alpha_{ca}F}\ln\left(\frac{i}{i_{0,ca}}\right) \quad (14)$$

$$V_{conc} = \frac{RT_{fc}}{2F}\ln\left(1 - \frac{i}{i_{lim}}\right) + \\ + \frac{RT_{fc}}{4F}\ln\left(1 - \frac{i}{i_{lim}}\right) \quad (15)$$

$$V_{ohm} = \frac{\delta}{\sigma} i \quad (16)$$

Table 1 - Electrolyzer and fuel cell model data [13-14].

Common Data		
T_{ref}	298.15	K
R	8.314	$J/mol.K$
F	96485	C/mol
δ	$50 * 10^{-4}$	cm
λ	20	-
E_0	1.229	V
n	2	-
Electrolyzer Model Data		
T_{el}	350	K
p_{H_2}	$30 * 10^5$	Pa
p_{O_2}	$30 * 10^5$	Pa
p_{H_2O}	$30 * 10^5$	Pa
α_{an}	0.5	-
α_{ca}	0.5	-
$i_{0,an}$	$2 * 10^{-5}$	A/cm^2
$i_{0,ca}$	$1 * 10^{-1}$	A/cm^2
i_{lim}	3	A/cm^2
E_{th}	1.481	V
Fuel Cell Model Data		
T_{el}	350	K
p_{H_2}	$1 * 10^5$	Pa
p_{O_2}	$1 * 10^5$	Pa
p_{H_2O}	$1 * 10^5$	Pa
α_{an}	0.7	–
α_{ca}	1.7	–
$i_{0,an}$	$3{,}5 * 10^{-2}$	$A/cm2$
$i_{0,ca}$	$1 * 10^{-1}$	$A/cm2$
i_{lim}	2	$A/cm2$

The cell polarization curve, displayed in Figure 3, is calculated using equation 17.

$$V_{cell} = V_0 - V_{act} - V_{conc} - V_{ohm} \quad (17)$$

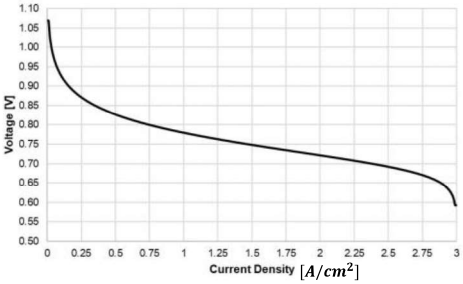

Figure 3–Modeled fuel cell, cell polarization curve.

3.2. Deviation

The components presented above will interact and the power balance, ΔP, will be determined. This operation is expressed in equation 18, where P_{gen} and $P_{T\ load}$ represent the total generation and load power respectively.

$$\Delta P = P_{gen} - P_{T\ load} \quad (18)$$

3.2.1. Equation of Motion

The equation of motion is used to represent the system's dynamic behavior [18]. This response is connected to the kinetic rotational energy stored in the rotating masses of synchronous generators,

expressed here in equation 21 [15-18], where J is the mass's moment of inertia and f_m is the machine's rotating frequency.

$$E_{kin} = \frac{1}{2} J(2\pi f_m)^2 \quad (21)$$

The inertia constant, H, is measured in seconds. With S_B being the generator's rated power, H can be calculated by equation 22. The values considered for H are in the range of $3 - 9\ s$ [6, 18-20].

$$H = \frac{E_{kin}}{S_B} = \frac{J\ (2\pi f_m)^2}{2S_B} \quad (22)$$

A synchronous system's response to a power imbalance is modeled with the equation of motion as a change in rotational frequency, $w_m = 2\pi f_m$. The machine's change in kinetic energy is expressed in equation 23 [20], $\frac{df_m}{dt}$ is the rate of change of said frequency and P_m and P_e are its mechanical and electrical powers.

$$\dot{E_{kin}} = J(2\pi)^2 f_m \left(\frac{df_m}{dt}\right) = \frac{2HS_B}{f_m}\left(\frac{df_m}{dt}\right) = (P_m - P_e) \quad (23)$$

The system response to a large power imbalance is the result of pooling the individual responses of all the machines in the grid. Each machine's frequency will approach the system's frequency as their individual dynamic response reaches an end, $f_m \longrightarrow f$. The individual inertia and rated power contributions, equation 24 and 25, are lumped together to define the system's characteristics.

$$S_{B_{sys}} = \sum_{\forall i} S_{B_i} \quad (24)$$

$$H_{sys} = \frac{\sum_{\forall i} H_i S_{B_i}}{S_{B_{sys}}} \quad (25)$$

The system's dynamic response can thus be modeled using equation 26, where f is the systems measured frequency and f_0 is its nominal frequency.

$$\frac{df}{dt} = \left(P_{gen} - P_{load}\right) \frac{f_0}{2H_{sys}S_{B_{sys}}} \quad (26)$$

3.2.2. Load Damping

In electrical systems some of the loads are dependent on the grid frequency. These loads have a positive impact on grid stability as they act as a damping mechanism. This effect is referred to as load damping, expressed in equation 28, where D is the load damping coefficient, Δf is the frequency deviation and ΔP is the resulting change in load. The value chosen for D in this model was $0.6\ MW/Hz$.

$$\Delta P = D\ \Delta f \quad (27)$$

3.3. Response:Droop Control

In the event of a considerable frequency deviation the system's reserves will be activated. In this model the system reserves refer to the synchronous or hydrogen system's capacity that is kept available to respond to power imbalances in the system. The reserves in this model are made to mimic the FCR in functioning and purpose.

The actual response to a frequency deviation is made separately by each technology. The electrolyzer system will work from the demand side, changing the amount of load it uses, while the synchronous generators and fuel cell systems will work from the supply side, altering the amount of power they produce. They will all use the same mechanism although with different bid values, a droop control mechanism, the standard for FCR. In droop control the change in operation point is performed through the engagement of a linear relationship between frequency deviation and power. The slope of this line is defined by a droop control characteristic, B, the frequency bias, expressed in equation 29, with P_{bid} corresponding to the capacity that was allocated for FCR, usually defined by the bid made, and Δf_{lim} to the set maximum frequency deviation, the point where the complete bid must be activated, $200\ mHz$ here. Systems working from the supply side will have a negative droop characteristic while ones working from the demand side will have a positive one.

$$B = \pm \frac{P_{bid}}{\Delta f_{lim}} \quad (28)$$

The reserve action, the change in power, is thus calculated using equation 30, where Δf is the frequency deviation, B is the frequency bias and ΔP is the resulting power change action of the reserve.

$$\Delta P = B\Delta f \quad (29)$$

3.4. Grid Model

The complete grid model, with all the connected systems is displayed in Figure 4, where its seen how the loads and the sources are summed inside their groups and a balance is made between their total instantaneous values. The resulting power imbalance, ΔP, will lead to a frequency deviation, Δf, that is calculated following the principles of the Equation of Motion. The frequency rate of change will drive the system frequency, f, away from its nominal value and the droop control loops will be used to adjust the power, through the system's reserves, and bring the system back into an equilibrium state.

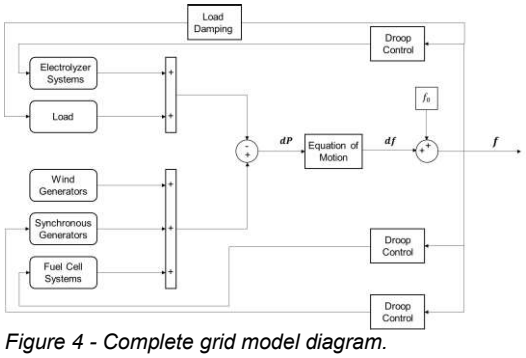

Figure 4 - Complete grid model diagram.

3.4.1. Model Limitations

This is a simplified model of an electric grid and its frequency dynamics, created in Matlab/Simulink. In this model no controllers were included, leading to limitations in simulating the transitional periods of power output of the reserves, which demonstrated overshoots followed by oscillations before settling down. Despite of this the model is capable of correctly simulating the focused behaviors of the system when responding to power imbalance, the initial power and frequency response, the performance of different parameters and the steady state reached after the system is stabilized.

3.4.2. Electrolyzer Equivalent Inertia

To compare the results obtained from the variations of model parameters a novel metric is introduced here. This uses the frequency deviation changes from increments in H and the electrolyzer power to estimate an equivalence between the two. The frequency deviations, Δf, are calculated with equation 31, where f represents the frequency at the peak of the deviation and f_0 is the nominal system frequency.

$$\Delta f = f_0 - f \tag{30}$$

The improvements in frequency deviations caused by increases in H and electrolyzer power, Δf_H and Δf_{Pel}, are estimated with equations 32 and 33, and the averages of those improvements, $\Delta f_{H_{avg}}$ and $\Delta f_{Pel_{avg}}$, with equations 34 and 35:

$$\Delta f_H = \Delta f(H_{i+1}) - \Delta f(H_i) \tag{32}$$

$$\Delta f_{Pel} = \Delta f(Pel_{i+1}) - \Delta f(Pel_i) \tag{33}$$

$$\Delta f_{H_{avg}} = \frac{1}{n}\sum \Delta f_H(i) \tag{34}$$

$$\Delta f_{Pel_{avg}} = \frac{1}{n}\sum \Delta f_{Pel}(i) \tag{35}$$

Those average values are then related to the change in electrolyzer power and H, ΔP_{el} and ΔH, through equations 36 and 37, respectively, resulting in the Impact of Electrolyzer Power, IEP, and the Impact of Inertia Constant, IIC.

$$IEP = \frac{\Delta f_{Pel_{avg}}}{\Delta Pel} \tag{36}$$

$$IIC = \frac{\Delta f_{H_{avg}}}{\Delta H} \tag{37}$$

The Electrolyzer Equivalent Inertia, EEI, calculated with equation 38, compares the impacts on frequency deviation, showing the amount of inertia needed to obtain the same improvement in frequency deviation as a certain amount of electrolyzer power.

$$EEI = \frac{IEP}{IIC} \tag{38}$$

4. Simulations and Results

With the purpose of understanding the influence of different grid parameters and the potential impact of hydrogen-technologies on frequency control, two sets of simulations were performed. The first set focuses on the frequency behavior after large power imbalances, and the second on the frequency behavior along a day with steady-state imbalances. On both scenarios the simple configurations and the hydrogen configurations will be tested.

4.1. Simulation set 1 – large disturbance response

This simulation set focuses on the initial frequency and FCR responses to large imbalances. The simulations will last 30 seconds. At the beginning of that period both power supply and demand will be set to 30 MW, then at second 5, a 5 MW step increase in load will be added. The Frequency Nadir (FN) and the Rate of Change of Frequency (RoCoF) will be measured, calculated respectively with equation 39 and 40.

$$FN = \min(f) \tag{39}$$

$$RoCoF = f(5.5) - f(5) \tag{40}$$

The starting point for the size of reserve is 8 MW in the case of Terceira Island [26].

4.1.1. Inertia Constant

Simulations were made with multiple values of H. In Figure 5 the profiles of power output and load, for an H of 6 seconds, are presented.

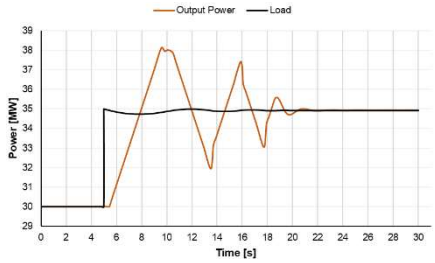

Figure 5 – Grid load and power output after a large disturbance for an H of 6, and FCR of 8 MW of synchronous power

It can be seen the effect of the model limitations, causing an overshoot of the synchronous machine's response. Besides that, on the load curve, the effect of load damping is apparent, changing the power

demand according to the frequency value. The corresponding frequency profile and others between the inertia values of 3 and 9 seconds, are presented in Figure 6. Additionally, the values of FN and RoCoF for these simulations are presented in Figure 7.

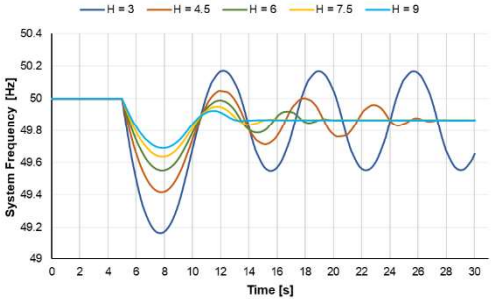

Figure 6 – Frequency profiles after a large disturbance for multiple values of H, for an FCR of 8 MW of synchronous power.

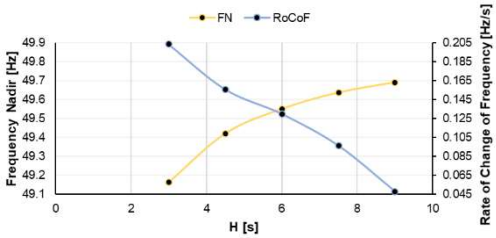

Figure 7-FN and RoCoF values for multiple values of H.

As can be seen in both figures, the amount of inertia in the system heavily affects the systems' frequency response, through both the FN and the RoCoF. Low levels of inertia show greater frequency deviations and larger RoCoF, and increasing inertia lowers these values linearly for the RoCoF but at an increasingly smaller rate for the FN.

4.1.2. Electrolyzer Configuration

The addition of the hydrogen technology plans to take advantage of its faster response times to help improve the system's response, 0.1 seconds, four times faster than synchronous machines [24]. The electrolyzer will thus function at a percentage of its maximum power to have the option of increasing or decreasing its power demand. This can be observed in Figure 8, which shows a 1 MW electrolyzer power profile during the response to the frequency deviation, with H equal to 6 and 8 MW of synchronous power in the FCR.

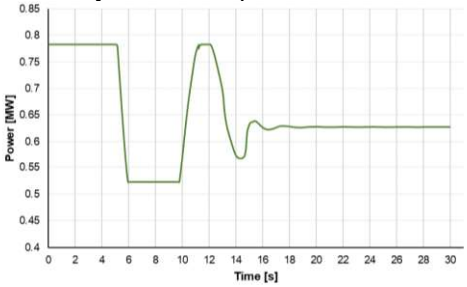

Figure 8 - Electrolyzer power output for a 25 percent bid window of a 1 MW electrolyzer.

Multiple simulations were performed for various amounts of electrolyzer power at different values of inertia constant. The results showed how the addition of electrolyzers does not affect the RoCoF in a considerable way, but it does affect the FN. The FN results of these simulations are presented in Figure 9. During all these simulations the amount of synchronous power in the FCR was kept at 8 MW and the inertia constant at 6 seconds. The growth of electrolyzer power, like the system's inertia, benefits the frequency stability but in a different way. Across all levels of inertia values tested, the marginal FN benefit achieved from increasing electrolyzer power was equal, but with the increase of system inertia, the impact on FN of increasing electrolyzer power is diminished.

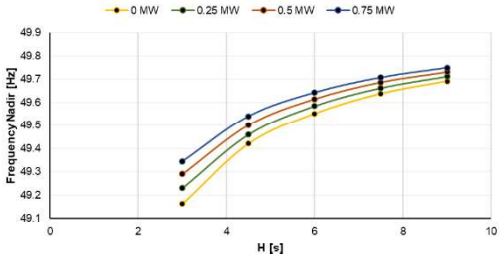

Figure 9-FN for values of electrolyzer power and H.

The EEI metric, presented in Section 3.4.2. was developed to relate the impacts of these two model parameters. Analyzing the results obtained, the EEI value was calculated for low levels and high levels of inertia, due to the non-linear behavior of this, resulting in 0.958 s/MW at low levels of inertia and 2.262 s/MW at high levels o inertia.

4.1.3. Fuel Cell Configuration

The fuel cell systems are only used to output more power, for that reason they are kept at standby, considered to be 5% of their maximum power.

With the positive frequency stability impact demonstrated by the electrolyzer configuration, the possibility of substituting FCR synchronous power with hydrogen-based power was tested. These simulations kept the size of FCR at 8 MW but substituted increasing amounts of synchronous power with equal amounts of hydrogen power. The results of this simulations are presented in Figure 10, displaying the simulation results of using just electrolyzer and of using fuel cells and electrolyzers, with equal shares.

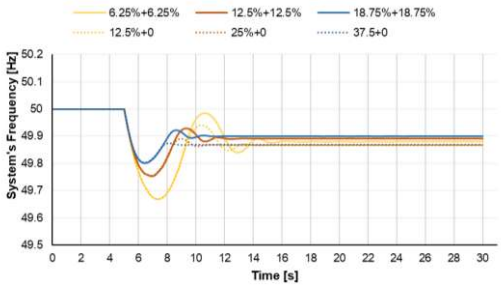

Figure 10 – Frequency profile for multiple combinations of fuel cell's and electrolyzer's power with equal participation in the Frequency Containment Reserve.

These results showcase the benefit in substituting shares of the FCR with hydrogen-based power, but also do not show considerable differences between the electrolyzer and the fuel cell configurations. Additionally, Figure 11, shows the power profiles of electrolyzer and fuel cell, in both the electrolyzer and fuel cell configurations. These systems have a 1 MW capacity, but function differently. The change in electrolyzer behavior between the two configurations is very slim.

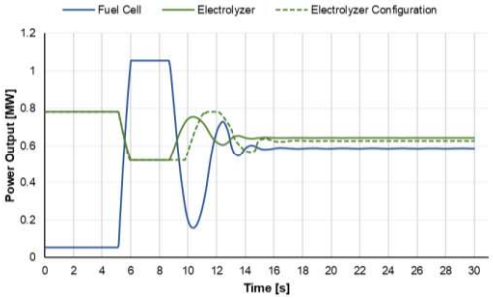

Figure 11 - Fuel cell and electrolyzer power outputs, for a 1 MW electrolyzer with a bid window of 25 percent, and a 1 MW fuel cell with a 95 percent bid window.

4.2. Simulation set 2 – steady-state imbalances

The second simulation set focused on the system's frequency behavior along a day without large power imbalances but with steady-state imbalances caused by load and wind power forecasting errors. The load data used is from 2012, with 4 days being chosen due to their varied power profiles, a Summer and Winter Wednesday and a Summer and Winter Sunday. The steady state imbalances were calculated using a percentage of the load, expressed in equation 42 for a 1% forecasting error.

$$P_L = P_{L\,forecast} * \left(1 + rand(-0.01; 0.01)\right) \quad (42)$$

The power profiles for the Summer Wednesday are displayed in Figure 12, including the load and wind power data, and the calculated synchronous power.

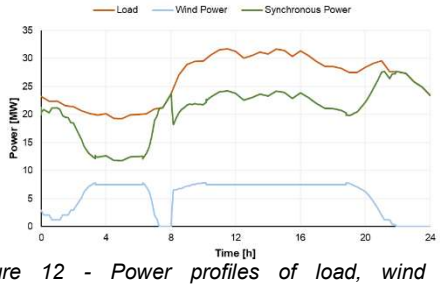

Figure 12 - Power profiles of load, wind and synchronous power along the Summer Wednesday.

The frequency profile for that day is presented in Figure 13. There are times with large variation spikes caused by the wind power, to avoid the effects of those the analysis the period between 12:00 and 16:00 was selected.

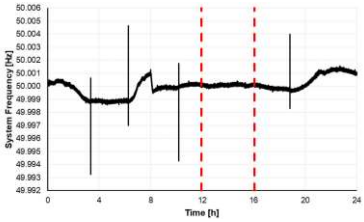

Figure 13 - System frequency along the Summer Wednesday with 1 percent steady-state imbalances.

4.2.1. Steady-state Imbalances

Simulations were made to analyze the impact on frequency stability of the size of steady-state imbalances. Testing values of steady-state imbalances of 1% and 5% of the load and wind power output, demonstrated in Figure 14, the results for the Summer Wednesday, show how increased uncertainty results in larger frequency envelopes, 3 times larger on average, and more erratic frequency variations, the same behavior was present in the other days.

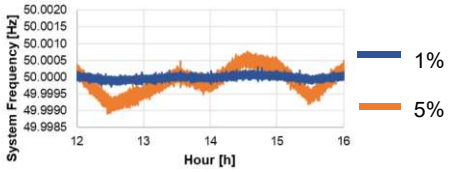

Figure 14 -System frequency for a Summer Wednesday during the 12:00 – 16:00 hour period, comparing the results with steady-state imbalances of 1 and 5 percent.

4.2.2. Electrolyzer Configuration

The hydrogen configuration was tested for a 1 MW hydrogen system with a deadband of 10 mHz. Due to the similar behavior achieved by the fuel cell configuration, only the electrolyzer configuration is displayed here. The simulations covered the system's frequency in each of the four selected days when the electrolyzer system is added and used to react to the steady-state imbalances, with the 1% value being applied. The results obtained for the Summer Wednesday are presented in Figure 15, with the results from the hydrogen configuration being displayed over the ones with the simple configurations. The remaining simulations showed similar

results. All simulations showed the hydrogen configuration improved results, keeping the system's frequency inside a narrower band.

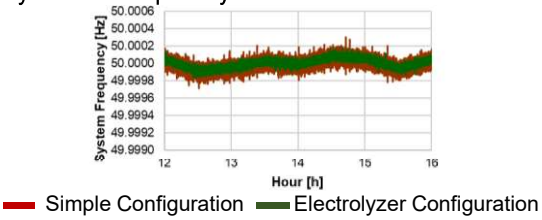

Figure 15-System frequency for a Summer Wednesday on the 12:00-16:00 hour period for the simple and the electrolyzer configurations, for 1% steady-state imbalances.

The exemplary electrolyzer power profile for the simulated Summer Wednesday is presented in Figure 16, showing constant changes in power that despite being small could reduces the stacks lifespan.

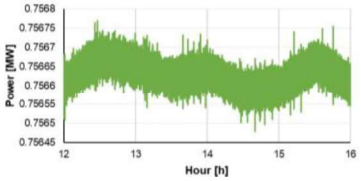

Figure 16 - Electrolyzer power profile along the simulated Summer Wednesday, for an electrolyzer of 1 MW with a 25 percent bid window, when responding to 1% steady-state imbalances.

Looking at the small improvements caused in the electrolyzer configuration and the electrolyzer profile, the question of balancing the benefits in grid frequency stability and the electrolyzer's lifespan must be asked.

5. Conclusions

Here a model of the electrical grid of the Terceira Island was developed. This model used load and wind speed data, together with developed models of synchronous generators and hydrogen-based technologies, electrolyzers and fuel cells. Based on the application of the equation of motion, the system's frequency behavior was simulated for situations of large power imbalances and steady-state imbalances, together with the system's response to that behavior, based on droop control mechanisms. The purpose was to understand the relevance of system's inertia and of the size of steady-state imbalances, on the current configuration of the island. From there, additional simulations were performed with the addition of electrolyzers and fuel cell systems to measure and evaluate their impact on frequency stability.

Two sets of simulations were done. The first focusing on the system's response to large disturbances and the second on the response to steady-state imbalances. The results clarified the influence of system inertia on the frequency stability of the system, showing how lower levels of inertia lead to increased frequency deviations and increased rates of change of frequency. Additionally, increased uncertainty in the forecasting of load and wind power showed to result in more pronounced frequency variations, across all the tested day.

The presence of hydrogen-based systems showed positive results in both scenarios, effectively and consistently decreasing the reached frequency nadirs, and decreasing the frequency envelope along the day. The new presented metric indicated an equivalence between the frequency deviation results of inertia and electrolyzer power to be 0.958 s/MW for levels of inertia between 3 seconds and 6 seconds, and 2.262 s/MW for higher levels, between 6 seconds and 9 seconds.

Further work on this topic must be done in the direction of understanding the economic benefits of hydrogen technologies providing grid services, the mechanisms that can be developed to make their introduction more feasible, as well as the environmental impacts of the substitution of synchronous carbon-based power sources in the frequency control services with hydrogen-based alternatives. Another direction of research is to clearly define, from the perspective of the hydrogen technologies, what are the potential benefits of each competing application, as, for example, the production of hydrogen, the storage of curtailed renewable energy or the provision of grid services.

6. References

[1] Carreiro, A. M., Oliveira e Silva, G., Vasconcelos, J. V., (2020). Estratégia Açoriana para a Energia 2030, Direção Regional da Energia - Governo Regional dos Açores.

[2] J. Widén *et al.*, "Variability assessment and forecasting of renewables: A review for solar, wind, wave and tidal resources," *Renewable and Sustainable Energy Reviews*, vol. 44. Elsevier Ltd, pp. 356–375, Apr. 01, 2015.

[3] S. Simoes, J. Seixas, P. Fortes, L. Dias, J. Gouveia, and B. Mauricio, "The Medium to Long-Term Role of Renewable Energy Sources in Climate Change Mitigation in Portugal," in *Proceedings of the World Renewable Energy Congress – Sweden, 8–13 May, 2011, Linköping, Sweden*, Nov. 2011, vol. 57, pp. 724–731.

[4] M. Joos and I. Staffell, "Short-term integration costs of variable renewable energy: Wind curtailment and balancing in Britain and Germany," *Renew. Sustain.*

Energy Rev., vol. 86, pp. 45–65, Apr. 2018.
[5] L. V. Villamor, V. Avagyan, and H. Chalmers, “Opportunities for reducing curtailment of wind energy in the future electricity systems: Insights from modelling analysis of Great Britain,” *Energy*, vol. 195, p. 116777, Mar. 2020.
[6] P. Makolo, R. Zamora, and T. T. Lie, “The role of inertia for grid flexibility under high penetration of variable renewables - A review of challenges and solutions,” *Renew. Sustain. Energy Rev.*, vol. 147, p. 111223, Sep. 2021.
[7] M. Koller, T. Borsche, A. Ulbig, and G. Andersson, “Review of grid applications with the Zurich 1 MW battery energy storage system,” *Electr. Power Syst. Res.*, vol. 120, pp. 128–135, Mar. 2015.
[8] A. A. Solomon, D. M. Kammen, and D. Callaway, “Investigating the impact of wind-solar complementarities on energy storage requirement and the corresponding supply reliability criteria,” *Appl. Energy*, vol. 168, pp. 130–145, Apr. 2016.
[9] C. Chen, Y. Lu, and L. Xing, “Levelling renewable power output using hydrogen-based storage systems: A techno-economic analysis,” *J. Energy Storage*, vol. 37, p. 102413, May 2021.
[10] F. Alshehri, V. G. Suárez, J. L. Rueda Torres, A. Perilla, and M. A. M. M. van der Meijden, “Modelling and evaluation of PEM hydrogen technologies for frequency ancillary services in future multi-energy sustainable power systems,” *Heliyon*, vol. 5, no. 4, p. e01396, Apr. 2019.
[11] R. Bhandari, C. A. Trudewind, and P. Zapp, “Life cycle assessment of hydrogen production via electrolysis - A review,” *J. Clean. Prod.*, vol. 85, pp. 151–163, 2014.
[12] M. Shaygan, M. A. Ehyaei, A. Ahmadi, M. E. H. Assad, and J. L. Silveira, “Energy, exergy, advanced exergy and economic analyses of hybrid polymer electrolyte membrane (PEM) fuel cell and photovoltaic cells to produce hydrogen and electricity,”*J. Clean.Prod.*,vol.234,p.1082-1093,Oct.2019.
[13] M. El-Shafie, S. Kambara, and Y. Hayakawa, “Hydrogen Production Technologies Overview,” *J. Power Energy Eng.*, vol. 07, no. 01, pp. 107–154, 2019.
[14] J. Chi and H. Yu, “Water electrolysis based on renewable energy for hydrogen production,” *Cuihua Xuebao/Chinese Journal of Catalysis*, vol. 39, no. 3. Science Press, pp. 390–394, Mar. 01, 2018.
[15] J. Milewski, J. Kupecki, A. Szczęśniak, and N. Uzunow, “Hydrogen production in solid oxide electrolyzers coupled with nuclear reactors,” *Int. J. Hydrogen Energy*, vol. 46, no. 72, pp. 35765–35776, Oct. 2021.
[16] D. S. Falcão and A. M. F. R. Pinto, “A review on PEM electrolyzer modelling: Guidelines for beginners,” *Journal of Cleaner Production*, vol. 261. Elsevier Ltd, p. 121184, Jul. 10, 2020.
[17] Z. Abdin, C. J. Webb, and E. M. A. Gray, “PEM fuel cell model and simulation in Matlab–Simulink based on physical parameters,” *Energy*, vol. 116, pp. 1131–1144, Dec. 2016.
[18] R. Eriksson, N. Modig, and K. Elkington, “Synthetic inertia versus fast frequency response: A definition,” in *IET Renewable Power Generation*, Apr. 2018, vol. 12, no. 5, pp. 507–514.
[19] P. Tielens and D. Van Hertem, “The relevance of inertia in power systems,” *Renew. Sustain. Energy Rev.*, vol. 55, pp. 999–1009, Mar. 2016.
[20] A. Ulbig, T. S. Borsche, and G. Andersson, “Impact of low rotational inertia on power system stability and operation,” *IFAC Proc. Vol.*, vol. 19, pp. 7290–7297, 2014.
[21] A. Ulbig, T. S. Borsche, and G. Andersson, “Analyzing Rotational Inertia, Grid Topology and their Role for Power System Stability,” *IFAC-PapersOnLine*, vol. 48, no. 30, pp. 541–547, Jan. 2015.
[22] Y. Cheng, R. Azizipanah-Abarghooee, S. Azizi, L. Ding, and V. Terzija, “Smart frequency control in low inertia energy systems based on frequency response techniques: A review,” *Appl. Energy*, vol. 279, p. 115798, Dec. 2020.
[23] B. C. Ummels, “Power System Operation with Large-Scale Wind Power in Liberalised Environments,” pp. 1–193, 2009.
[24] M. Virji, G. Randolf, M. Ewan, and R. Rocheleau, “Analyses of hydrogen energy system as a grid management tool for the Hawaiian Isles,” *Int. J. Hydrogen Energy*, vol. 45, no. 15, pp. 8052–8066, 2020.
[22] IEA (2020), Renewable Power, IEA, Paris https://www.iea.org/reports/renewable-power
[23] IEA (2020), Tracking Power 2020, IEA, Paris https://www.iea.org/reports/tracking-power-2020
[24] IEA (2020), Renewable Power, IEA, Paris, https://www.iea.org/reports/renewable-power
[25] SOLCAST, https://solcast.com/
[26] Guzzi, F., 2016, Development of a modelling and planning tool for renewable microgrids: The case study of Terceira Island, Master Thesis, Instituto Superior Técnico, Lisbon